Vrije Universiteit Brussel

VUB VRIJE UNIVERSITEIT BRUSSEL

Aerospace-grade surface mounted optical fibre strain sensor for structural health monitoring on composite structures evaluated against in-flight conditions

Goossens, Sidney Frans; De Pauw, Ben Dieter; Geernaert, Thomas; Salmanpour, M.S.; Sharif Khodaei, Z.; Karachalios, E.; Saenz-Castillo, D.; Thienpont, Hugo; Berghmans, Francis

PAPER • OPEN ACCESS

Aerospace-grade surface mounted optical fibre strain sensor for structural health monitoring on composite structures evaluated against in-flight conditions

Aerospace-grade surface mounted optical fibre strain sensor for structural health monitoring on composite structures evaluated against in-flight conditions

Sidney Goossens[1,2] , Ben De Pauw[1,2] , Thomas Geernaert[1,2] ,
Mohammad Saleh Salmanpour[3], Zahra Sharif Khodaei[3],
Evangelos Karachalios[4], Diego Saenz-Castillo[5] , Hugo Thienpont[1,2] and
Francis Berghmans[1,2]

[1] Vrije Universiteit Brussel, Department of Applied Physics and Photonics, Brussels Photonics, Pleinlaan 2, B-1050 Brussel, Belgium
[2] Flanders Make, Oude Diestersebaan 133, B-3920 Lommel, Belgium
[3] Imperial College London, Department of Aeronautics, South Kensington Campus, Exhibition Road, SW7 2AZ London, United Kingdom
[4] Hellenic Aerospace Industry, Engineering Research Design and Development Directorate, 32009 Shimatari, Greece
[5] FIDAMC, Foundation for the Research, Development and Application of Composite Materials. Avda. Rita Levi Montalcini 29, Tecnogetafe, E-28906 Getafe, Madrid, Spain

E-mail: sidney.goossens@vub.be

CrossMark

Abstract

Optical fibre sensors are being investigated since many years as candidates of choice for supporting structural health monitoring (SHM) in aerospace applications. Fibre Bragg grating (FBG) sensors, more specifically, can provide for accurate strain measurements and therefore return useful data about the mechanical strain state of the structure to which they are attached. This functionality can serve the detection of damage in an aircraft structure. However, very few solutions for protecting and bonding optical fibres to a state-of-the-art aircraft composite material have been reported. Most proof-of-principle demonstrations using optical fibre sensors for aerospace SHM-related applications reported in literature indeed rely on unpackaged fibre sensors bonded to isotropic metallic surfaces in a mostly unspecified manner. Neither the operation of the sensor, nor the adhesive material and bonding procedure are tested for their endurance against a full set of standardized in-flight conditions. In this work we propose a specialty coated FBG sensor and its permanent installation on aerospace-grade composite materials, and we demonstrate the compatibility with aerospace in-flight conditions. To do so we thoroughly evaluate the quality of the operation of the FBG sensor by correlating the reflection spectra of the installed sensors before and after exposure to a full set of realistic in-flight conditions. We also evaluate the difference in strain measured by the FBG, since any damage in the adhesive bond line would lead to strain release. The applied test conditions are based on aerospace standards and include temperature cycling, pressure cycling, exposure to humidity and

hydraulic fluid and fatigue loading. We show that both the bond line and the quality of the sensor signal were negligibly affected by the applied environmental and mechanical loads representing in-flight conditions and therefore conclude that it can be considered for SHM of aerospace-grade composite materials.

Keywords: structural health monitoring, fibre Bragg grating, composite materials, aerospace, optical fibre sensors, sensor qualification

(Some figures may appear in colour only in the online journal)

1. Introduction

Composites are rapidly replacing metals in aerospace structures, essentially owing to their higher stiffness-to-mass ratio. However, their proneness to impact damage calls for frequent inspection, which in its turn increases downtimes and operational costs. An integrated sensor network, allowing for permanent non-destructive evaluation that can support structural health monitoring (SHM), could overcome these issues and be more cost-efficient [1]. Optical fibre sensors have long been considered as ideal candidates for that purpose, owing to their small size, low weight, immunity to electromagnetic interference and multiplexing capabilities [2]. Fibre Bragg gratings (FBGs) in particular, have been commonly used as precise and accurate strain sensors. Several studies have proven their superiority to electrical strain gages (ESGs) in terms of fatigue and durability [3–5]. An FBG is a local and periodic refractive index perturbation in the core of a single mode optical fibre that reflects a narrow spectral band centred around the so-called Bragg wavelength. The Bragg wavelength shifts linearly with temperature and strain variations, as explained in more details in section 2.1. Measuring the wavelength shift therefore allows determining the mechanical strain at the location of the FBG. An accurate measurement of the strain nevertheless requires adequate quality of the FBG reflection spectrum and suitable signal acquisition hardware as well as adapted data-processing methods.

The small size of optical fibres allows them to be embedded in between the plies of a composite panel. Several reports in literature project that embedding the optical fibre in the direction of the reinforcement fibres yields negligible influence on the mechanical and fatigue properties of the composite [6–10]. The occurrence of resin pockets around an embedded optical fibre, for example, can be minimized by doing so. However, and while embedding actually also protects the optical fibre from the environment, there are still concerns that the ingress and egress locations of the fibre at the edges of a composite panel could act as damage initiators and locally affect the strength of the composite. These locations can usually not be chosen with great flexibility, which, together with the need to align the optical fibre with the reinforcement fibres, also limits the flexibility in terms of selecting the best placement of the sensors. In addition, such ingress and egress points are not readily compatible with the

different manufacturing and machining steps of aerospace-grade composite components.

Surface mounted optical fibre sensors, on the other hand, can be bonded after completing manufacturing of the composite component. This allows for more flexibility in choosing the best location for the sensor and gives better prospects for repairing or replacing a damaged sensor. However, when they are not protected by the composite itself, they typically require additional protection from the environment [2].

For use of permanently installed FBGs in aerospace applications, the fibre must be protected by a suitable coating or a jacket and attached with an adequate adhesive. Indeed even when only on-ground SHM inspection methodologies are considered, the FBGs should be installed in such a way that the required sensor functionality is not compromised as a result of the in-flight conditions. Furthermore, installation and handling must be made as flexible and repeatable as reasonably achievable.

Only very few dedicated mounting and bonding techniques for optical fibre sensors, and FBGs in particular, have been investigated in this respect. One possibility for protecting the optical fibre sensor is to sandwich it between two prepreg layers of carbon or glass reinforced polymer [11, 12]. A commercial example hereof is the HBM FS62-17 composite strain sensor [13].

Another recent development is the fibre optic ribbon tape (FORT) [14, 15]. One embodiment of a FORT is a precured slab of two laminas of glass/epoxy woven fabric prepreg, with an embedded optical fibre coated with polyimide. The FORT can be mounted through secondary bonding or during co-curing. The reliability of FBG-based sensors, mounted using both bonding methods, was compared to that of mounted ESGs during a fatigue 3-point bending test of 10^6 cycles at 1 kN and assessed against numerical results. The FORT signals correlated highly with the expected results and outperformed the ESGs, which started drifting after 6.4×10^5 cycles, presumably due to debonding or metal fatigue.

While these, and other studies [16, 17] deal with the need for protecting and bonding optical fibre sensors, these solutions usually lack versatility in mounting. Indeed, precured two-dimensional slabs cannot be bonded with a surface featuring corners, grooves or with even more complex three-dimensional shapes. While the FORT offers the ability to be co-cured while manufacturing the host composite component,

this also sets limitations to the component's manufacturing process.

Furthermore, these techniques typically protect the fibre at the location of the sensor only. When multiplexing series of sensors along one optical fibre line, each sensor will have to be connected to the next by ways of an additional length of optical fibre spliced or connected to the sensor fibre. This connecting fibre should also be protected by a jacket or a coating and should be bonded with the surface. This also means that at least two splices or connectors are required per sensor, inducing additional losses and weak points in the sensor line.

Finally, so far only a limited set of the entire collection of harsh in-flight operational environment conditions have been addressed while testing the sensors. These were mostly limited to exposing the sensors to prescribed strain and temperature levels, since these are physical quantities that can be measured by the FBG and can be compared with other types of sensors. The susceptibility to other environmental in-flight conditions has mostly been disregarded.

In this work, we address these shortcomings, by proposing a solution based on an optical fibre equipped with draw-tower fibre Bragg gratings (DTG®) and coated with glass fibre reinforced polymer (GFRP) and high-density polyethylene (HDPE), named strain measurement wire (SMW) [18]. We attach this SMW to aerospace-grade composite using a dedicated epoxy adhesive-based mounting method. The one-dimensional nature of the wire allows for mounting the sensor under any angle regardless of the shape of the surface. The entire fibre is packaged and can therefore be bonded along its entire length with the composite surface, leaving no weak points along said length. Preliminary results already showed to be very promising [19].

We bonded the fibre with three kinds of aerospace-grade carbon fibre reinforced polymer (CFRP) materials and we exposed those to a set of in-flight conditions defined by ASTM International (formerly known as American Society for Testing and Materials) and RTCA (known as Radio Technical Commission for Aeronautics) standards. These conditions do not only include temperature and strain cycling, but also extreme and shock-like exposure to temperature, pressure and humidity, and exposure to vibrations, to hydraulic fluids and to tensile fatigue cycling.

To assess whether the sensors and the bonding method provide for adequate robustness against exposure to these harsh in-flight conditions, we compare the reflection spectra of the sensors after an environmental test to the spectra obtained before the test. We pay particular attention to the influence of bonding and of the environmental parameters on the quality of these spectra, as the latter are crucial in view of enabling high-accuracy strain measurements and vibration analysis-based damage identification in composite structures, such as acoustic emission or ultrasonic Lamb wave-based damage detection. We also investigate whether damage in the adhesive bond line or the SMW itself occurs by checking on the introduction of large strain releases or local non-uniform strain distributions around the grating-based sensor.

We structured our manuscript as follows. Section 2 introduces the properties of a fibre Bragg grating and how to quantify its quality and explains how such unpackaged grating-based sensor compares with its SMW and ribbon tape packaged counterparts. We also elaborate on the installation method for surface mounting the SMW onto the CFRP test coupons. Section 3 proceeds with explaining the in-flight condition test campaign and how these affect the reflection spectra. The conclusion is presented in section 4.

2. Materials and methods

2.1. FBGs

An FBG is a periodic modulation of the refractive index fabricated within the core of a single mode optical fibre which acts as a wavelength selective mirror that reflects a narrow spectral band centred around the so-called the Bragg wavelength, λ_b, proportional to the effective refractive index, n_{eff}, and the period, Λ, of the grating, as given by equation (1) [20, 21].

$$\lambda_b = 2\, n_{eff}\, \Lambda. \tag{1}$$

Depending on the length and the reflectivity of the grating, the reflection spectrum will have a bandwidth, measured as the full width at half maximum (FWHM), of typically 50–300 pm [22]. Figure 1 shows an example of a Bragg peak of one of the FBGs used in this work, with a λ_b of 1538.540 nm and an FWHM of 102 pm.

When a mechanical or thermal load is applied uniformly along the axis of the optical fibre, the grating is strained, and the effective index and period of the grating will change accordingly, resulting in a shift of the Bragg wavelength λ_b [23].

Typical SHM with FBGs on large structures, including composites, makes use of dynamic measurements, such as ultrasonic guided wave inspection (UGW) [24, 25], acoustic emission [26], modal analysis [27, 28]. In these cases, it becomes challenging to acquire the whole Bragg reflection spectrum. The change in Bragg wavelength is usually obtained by means of edge filtering: a narrow linewidth laser is tuned to the slope of the Bragg peak. When a strain is applied to the grating, a shift in Bragg peak will result in a linearly proportional change in reflected power, as illustrated in figure 1(b).

When a uniform axial strain is acting on the grating, the Bragg peak will shift proportionally, as exaggeratedly shown in figure 2(a). However, if a non-uniform strain is present over the length of the FBG, then the Bragg peak will no longer be perfectly symmetric around the Bragg wavelength, and the peak will be distorted [29]. This is schematically shown in exaggeration in figure 2(b). A non-uniform axial strain can be present due to damage or debonding in the fibre's coating, packaging or bonding method. As a result of the distortion, the left and right slope of the main Bragg reflection will be modified. If this compromises the availability of a steep and linear slope in the Bragg reflection
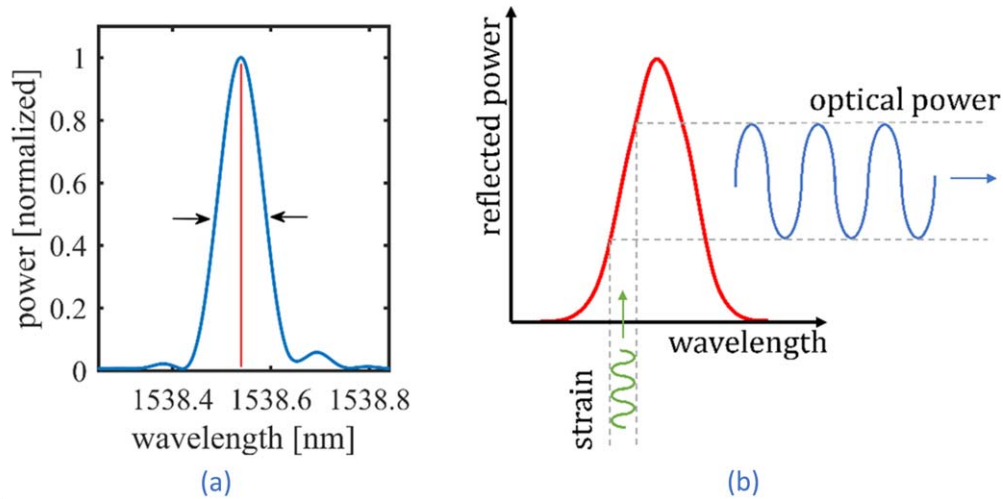
Figure 1. An example of an FBG reflection spectrum used in this work with a Bragg wavelength of 1538.540 nm marked with the red line, and an FWHM bandwidth of 102 pm denoted by the arrows (a), and edge filtering on a steep slope of an FBG spectrum allows for (linear) conversion of a dynamic strain signal into an optical power signal (b).
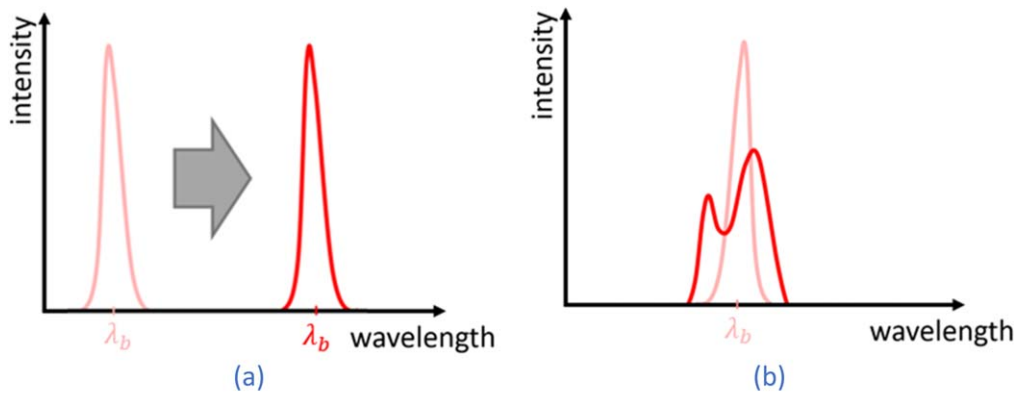

Figure 2. An exaggerated schematic representation of uniform strain along the FBG, yielding a wavelength shift (a) and an increase in non-uniform strain, yielding a distortion of the Bragg peak (b).

spectrum, the sensors response for edge filtering techniques will be accordingly affected.

In order to quantify the distortion of an FBG reflection spectrum, one can use several figures of merit, such as for example the asymmetry of the Bragg peak, the linearity of the slopes, the FWHM of the Bragg peak, The asymmetry of a Bragg peak measures how well the left edge coincides with the right edge, when either side is mirrored around Bragg wavelength, and is thus a measure for the distortion. The linearity of the slope is important for applied strain converting measured optical power. The FWHM of a Bragg peak is inversely related to the slope of the edge of the peak, as a lower FWHM will yield a steeper edge and thus higher strain to optical power amplification, as can be observed in figure 1(b).

For the analysis in the manuscript, these figures of merit can however be summarized into one parameter, namely the Pearson correlation coefficient. For two data sets of measured Bragg peak reflection spectra, x and y, the Pearson correlation can be defined as in equation (2), with x_i and y_i the individual data points of each spectrum, $\bar{x}$ and $\bar{y}$ their respective means

and n the number of data points in each set.

$$\rho(x, y) = \frac{\sum_{i=1}^{n}(x_i - \bar{x})(y_i - \bar{y})}{\sqrt{\sum_{i=1}^{n}(x_i - \bar{x})^2}\sqrt{\sum_{i=1}^{n}(y_i - \bar{y})^2}}. \qquad (2)$$

To evaluate the quality of a single Bragg peak, we correlate a reflection spectrum x with a mirrored version of itself, around the Bragg wavelength, and thus taking $y_i = x_{n-i+1}$ for $i = 1: n$. A value of $\rho = 100\%$ corresponds to a reflection spectrum that is perfectly symmetric around the Bragg wavelength. We will call this method the mirror correlation and use it in section 2.2 to quantify the amount of asymmetry present on a Bragg peak.

For investigating the effect of a certain exposure or load, we cross correlate the Bragg peak before the load, x, with the same peak after the load, y. A ρ-value of 100% means the reflection spectrum after the load is perfectly correlated with the spectrum of the Bragg peak before applying the load, and there was no increase in distortion or change in asymmetry. We will refer to this method as the cross correlation and use it instead in section 3.2 where we are mainly interested in the load-induced change of the Bragg peak spectrum.

2.1.1. Draw-tower-gratings. We used commercially available FBGs which are UV-written Draw Tower Gratings® (DTGs). These FBGs are inscribed immediately after drawing the optical fibre and before applying the protective polymer coating, which in this case is Ormocer® [30–32]. As a result, no coating needs to be removed prior to inscribing the FBGs, which in its turn provides these DTGs® with excellent strength and fatigue characteristics. DTGs® are therefore less likely to fail during installation and use. DTGs® can be easily fabricated in multiplexed chains within a single fibre. The centre-to-centre distance can be as small as ˜1 cm, whilst their spectral spacing can be chosen as a function of the required number of sensors per fibre and the spectral width of the sensor read-out equipment. Here we used 8 mm long DTGs® with reflectivity values of about 30 %. The eventual NDI application could use other grating lengths, depending on the envisioned method. The reported distortions will most likely be smaller for shorter gratings.

We interrogated the DTGs® in reflection through a circulator with a Santec TSL-710 semiconductor tunable laser at a sweeping speed of 10 nm s^{-1} delivering 5 – 20 mW of optical power within a spectral width ranging from 1480 to 1640 nm and a Thorlabs PDA20CS InGaAs photodiode sampled at 100 kHz by a TiePie HandyScope HS5. This combination provided for a spectral resolution of 1 fm. The absolute wavelength accuracy and repeatability of the tuneable laser at room temperature are specified to be ±1 pm.

When locking the lasing wavelength on the slope of such a DTG in a thermally stable environment, we observed fluctuations of 30 fm. This means that for this particular interrogation an accuracy of about 30 fm can be obtained, corresponding to a minimally detectable (residual) strain difference of 25 $n\varepsilon$.

2.2. Fibre package comparison

To select the best package for this application, we compared the quality of the reflection spectra of regular Ormocer® coated, but further unpackaged DTGs®, to that of two types of packaged DTG®s. The first is the ribbon tape fibre (RTF) that sandwiches a regular Ormocer-coated DTG® in between two layers of glass fibre reinforced plastic (GFRP) with a width of 9.90 mm, and a height of 0.35 mm and therefore resembles the FORT introduced earlier. The second is the Strain Measurement Wire (SMW) [18] that consists of regular Ormocer-coated DTGs® embedded in a wire-like cylindrical profile of GFRP of 1.0 mm diameter and equipped with a protective outer jacket of high-density polyethylene (HDPE) of 0.2 mm. The GFRP provides for mechanical robustness along the entire fibre length, i.e. not only at the location of the DTGs®, whilst the HDPE jacket prevents any humidity or oil ingress. The three DTG® types and their package are shown in figure 3.

We bonded the DTGs® to 4 CFRP coupons, with the same specification as material M1 in in table 1. We used commercially available X120 adhesive from HBM [33], an epoxy based two-component adhesive designed for use with optical fibres. It has a Young's modulus of 1.5 MPa, an

operational temperature range of −55 °C to +120 °C and a density of 1 g cm^{-3}. *We applied this adhesive over a length of* 4 cm *with the* 8 mm-*long DTGs® in the centre.* The RTF was mounted whilst applying pressure and pre-strain during curing of the adhesive. The amount of adhesive has to be sufficient to cover the entire area of the RTF, but not excessive to prevent non-uniform bonding and non-uniform strain transfer from the composite to the DTG® [14]. We mounted an unpackaged fibre on one side of all four CFRP coupons, while on the other side an RTF or an SMW was mounted. The FBG was centred in the middle of the coupons for all packaging types, as is illustrated in figure 4.

After installation of the sensors, we exposed the coupons to strain and temperature loads. First, we strained the coupons 4 times longitudinally up to 120 $\mu\varepsilon$ while measuring the Bragg wavelength shift and the coupon extension, after which we exposed the coupons to 4 cycles from room temperature to 110 °C.

The Bragg reflection spectrum of each DTG was acquired before and after installation and after exposure to each load. To quantify the quality of the spectrum, we calculated the mirror correlation of each individual spectrum by using the Pearson correlation coefficient in equation (2).

Figure 5 shows the averages of these correlations per packaging type in a bar graph. After installation, the unpackaged DTG and RTF show a drop in correlation from respectively 0.906 ± 0.030 and 0.916 ± 0.028 to 0.888 ± 0.04 and 0.886 ± 0.020. After applying strain or temperature loads to the specimens, the correlation of the RTF and DTG continue to decrease. The effect on the SMW however is negligible.

These experiments show that quality of the DTGs in the SMW are least affected by installation, mechanical straining and temperature loading. In addition, the rotational symmetric shape allows for versatile mounting on 3D surfaces, and even the possibility for automated mounting by e.g. a robot arm because of the linear nature of the wire, application and distribution of adhesive. Moreover, during these experiments we noted that the strain sensitivity of the SMW was comparable to that of the DTG (while that of the RTF was 17% lower). Finally, the SMW is commercially available, contrary to the RTF (to the best of our knowledge).

2.3. Installation method of the SMW

After selecting the SMW in combination with the X120 adhesive, the installation method was optimized, focusing on ease of handling and repeatability.

To remove any residual strains between the fibre and the GFRP coating, the SMW was first annealed by exposing it to temperature cycles. To do so five of the interrogated SMW DTGs were annealed in an oven and heated at 5 °C min^{-1} from RT to 100 °C, after which the temperature was kept constant for more than 10 h and then the oven was turned off and the SMWs gradually cooled back down to RT in about 2 h. The Bragg wavelengths were acquired every 2 min by a Micron Optics SM125 optical sensing interrogator. We observed a hysteresis effect when comparing the Bragg
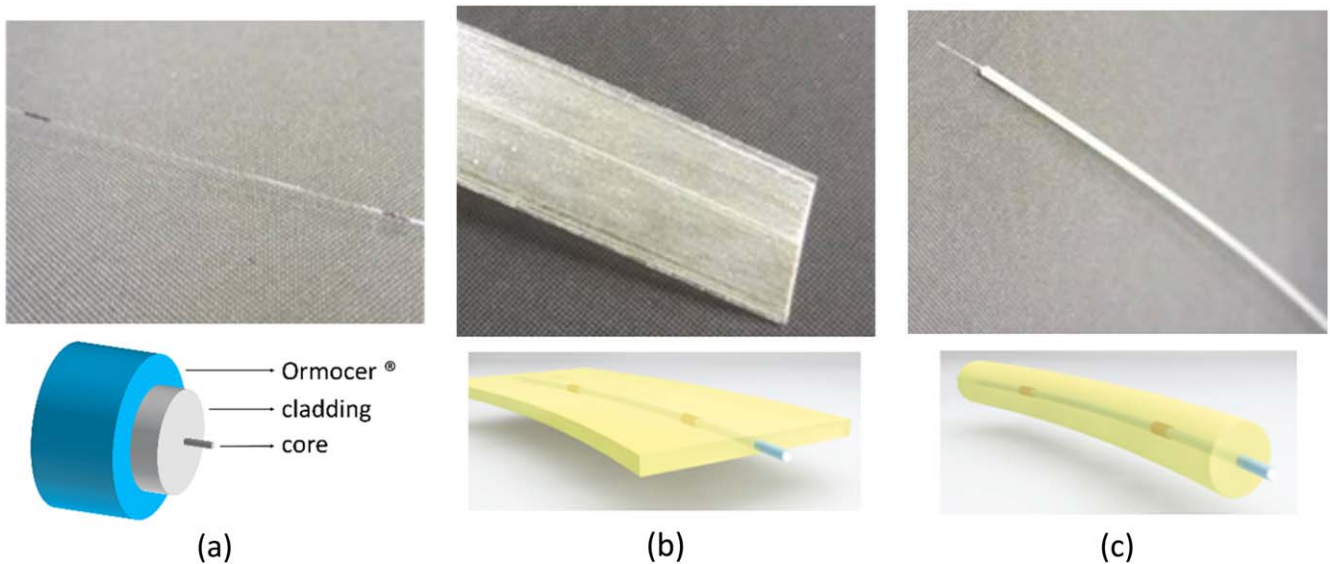
Figure 3. Pictures and illustrations of three DTG® versions: (a) unpackaged Ormocer® coated DTG®, (b) ribbon tape fibre and (c) strain measurement wire.

Table 1. Material properties of the three different types of CFRP coupons.

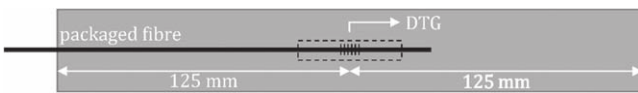| Reference	Type CFRP	Material	Stacking sequence	Thickness (mm)
M1	Unidirectional prepreg	M21/194/34%/T800S by Hexcel	[+45/-45/0$_2$/90/0]s	2.208
M2	Thermoplastic	Tenax®-E TPCL PEEK-HTA40	[0/90/+45/-45/0/90/+45/-45/0]	2.790
M3	M1 + CNT's	M21/194/34%/T800S by Hexcel + CNTs	[+45/-45/0$_2$/90/0]s	2.316

Figure 4. Schematic layout of a test coupon with an installed fibre, packaged either as an RTF or SMW (not shown), centering the 8 mm long DTG in the middle of the coupon. On the other side of each coupon an Ormocer® coated DTG was installed with the same geometry.

wavelength shifts during heating and cooling. The average Bragg wavelength shift, $\Delta\lambda_B$, of all five DTGs in function of the applied temperature is shown in figure 6 (a). A hysteresis is present in the first cycle and increases and changes slope in the second cycle, due to strain redistributions in the SMWs. Note that the ramp up of the 2nd cycle follows the ramp down of the 1st cycle. In the third cycle the slope remains similar, but the hysteresis reduces considerably.

We quantified the hysteresis by calculating the absolute enclosed surface (nm °C). These results are illustrated in figure 6(b). From cycle 1 to cycle 2 the hysteresis increases from on average 9.34 ± 0.93 nm °C to 17.43 ± 1.57 nm °C. In the third cycle the internal strain distribution relaxes, and the hysteresis reduces considerably to 1.83 ± 1.07 nm °C, and the SMW is ready for use.

To prepare the composite surface for applying the SMW, we first sand the surface mechanically, removing any resin surplus and subsequently clean and degrease with an alcohol solution. We then pre-strain the SMW (approx. 40 $\mu\varepsilon$), to
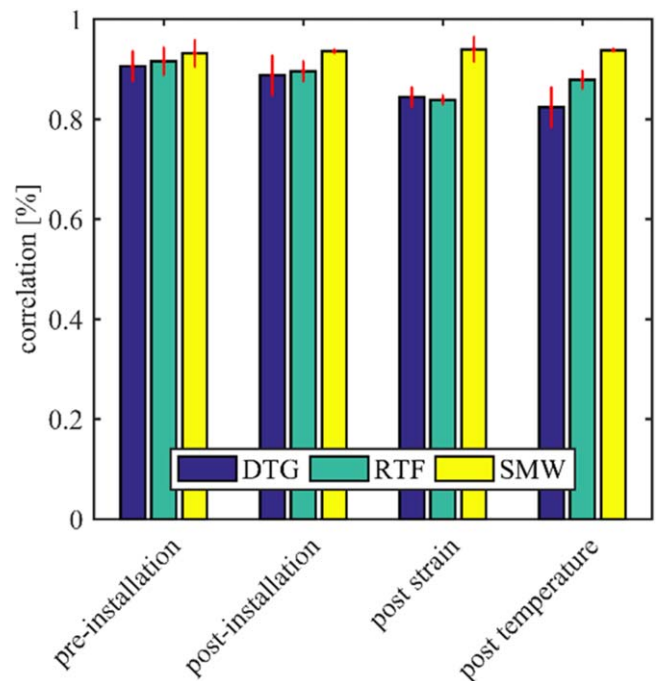
Figure 5. Mirror correlation of the Bragg peak reflection signals in the 3 considered packaging options at different stages of the comparative test.
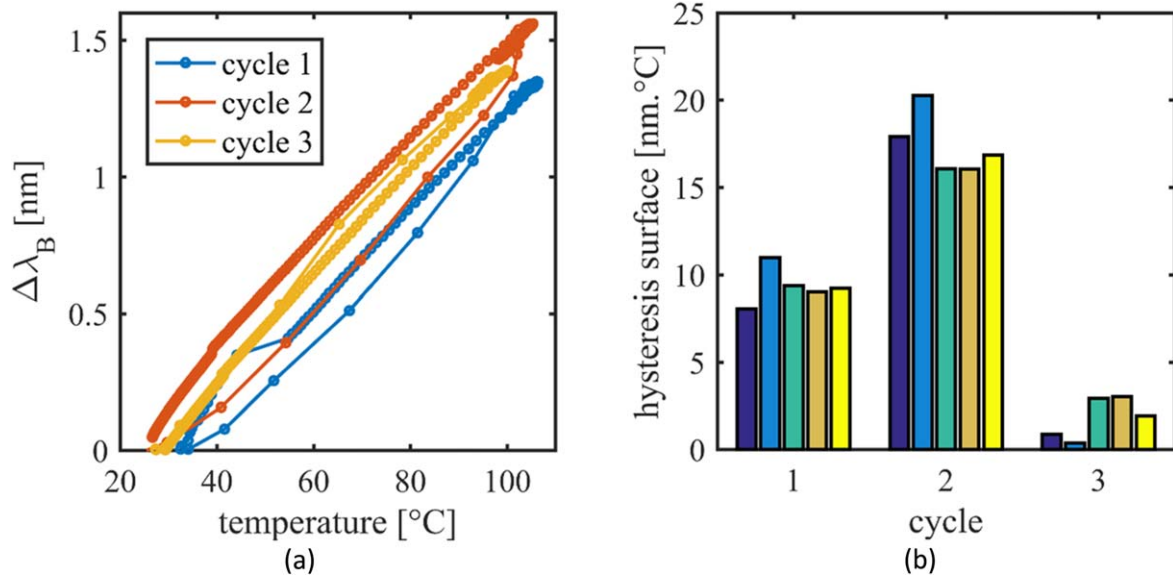
Figure 6. Average Bragg wavelength shift of the 5 tested DTGs versus temperature during thermal cycling (a); the calculated hysteresis value of the Bragg wavelength shift for all 5 DTGs per thermal cycle (b).
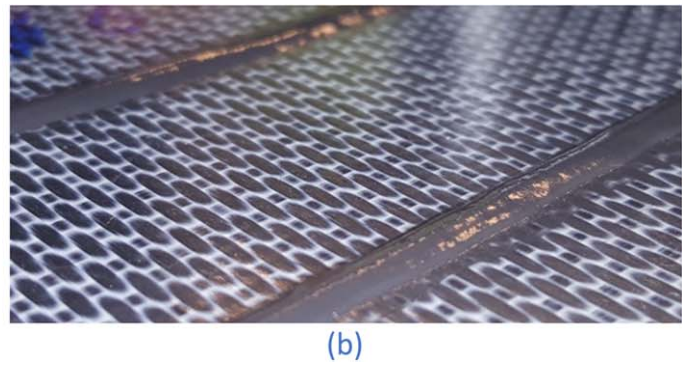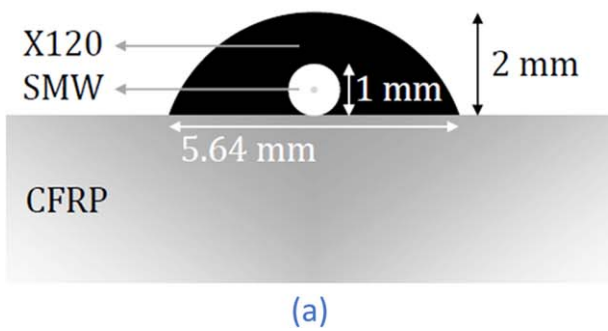
Figure 7. Schematic representation of the cross section of a SMW on a CFRP surface (a) and a picture of the result of two surface mounted SMWs on a thermoplastic CFRP coupon (b).
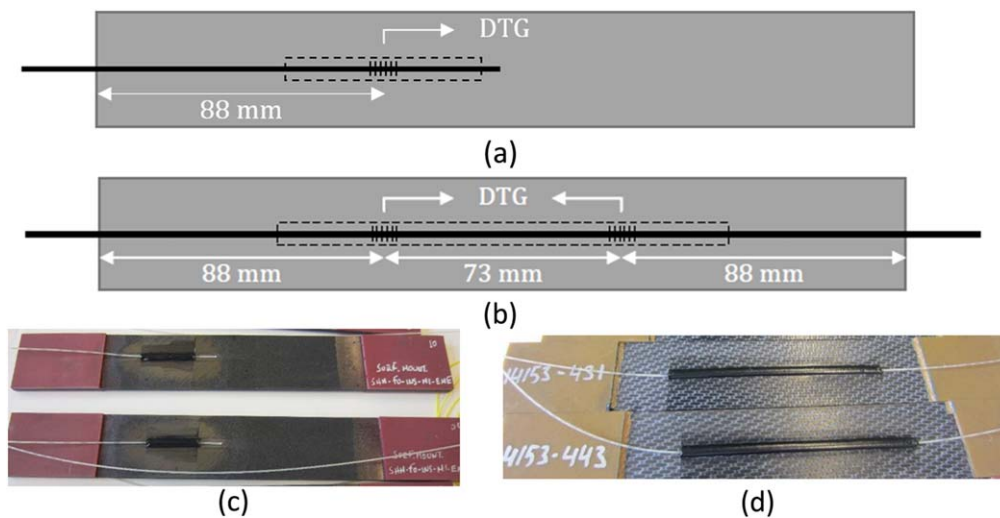
Figure 8. Overview of the coupons with surface mounted SMWs. The schematic of M1 and M3 coupons with 1 DTG per coupons (a), M2 with 2 DTGs per coupons (5) and a picture of two M1 coupons (c) and two M2 coupons (d).

(a) temperature load profile

(b) pressure load profile

(c) relative humidity load profile

(d) vibration load profile
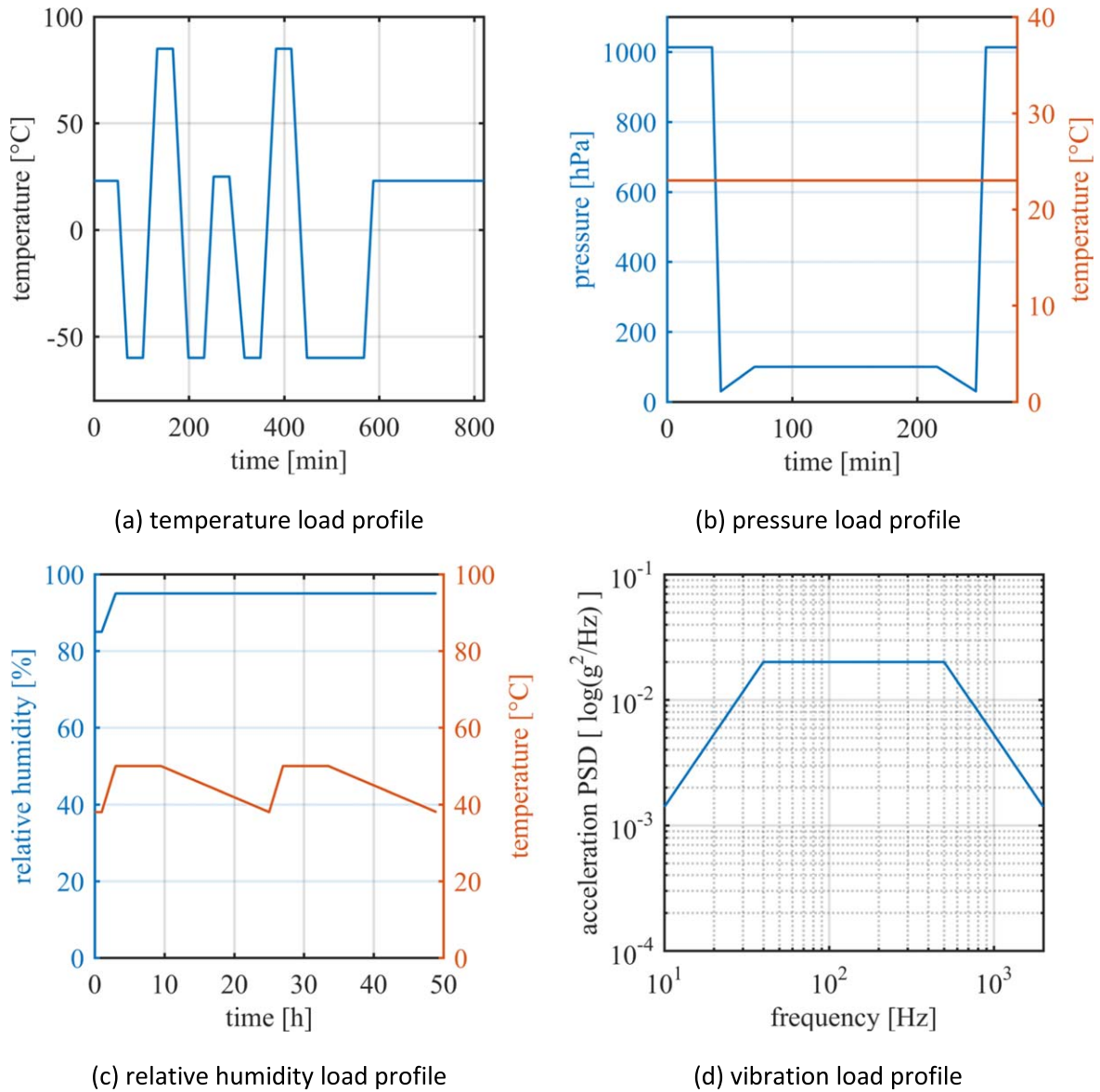
Figure 9. Environmental load profiles for temperature (a), pressure (b), relative humidity (c) and vibration (d).

Table 2. Tests, standards and parameters for in-flight conditions.

Test	Standard	Parameters	Equipment
Temperature	RTCA DO-160-4.0	low ($-60\,°C$)	TAC J2235 thermal vacuum camber
	RTCA DO-160-5.0	high ($+85\,°C$)	
		shock ($-60 \rightarrow +85\,°C$ in 33 min)	
Pressure		sea level (1013 hPa)	
		altitude of 47.000 ft (100 hPa)	
		shock ($1013 \rightarrow 30$ hPa in 15 min)	
Humidity	RTCA DO-160-6.0	RH $>90\,\%$ for 48 h	
		$50 \rightarrow 38\,°C$ ($<1\,°C\,h^{-1}$)	
Fluid susceptibility	RTCA DO-160-11.0	24 h submersed in aerosol	AeroShell fluid 41
Vibration	RTCA DO-160-8.0	random vibration APSD for 1 h	shaker
Tensile fatigue	ASTM D3479M	10^6 cycles of 5 kN ($R = 0.1$) at 5 Hz	Instron 8032 100 kN

Table 3. Summarized results for the in-flight conditions tests, showing the wavelength shift and Pearson cross correlation.

No.	Mat.	Test sequence applied	#DTGs	$\Delta\lambda$(pm)	σ(pm)	ρ(%)	σ(%)
1	M1	(a) Temperature test (b) Altitude test	2	116	±14	99.94	±0.01
2	M1	(a) Temperature test (b) Altitude test (c) Vibrational test	2	62	±24	99.99	±0.00
3	M1	(a) Temperature test (b) Altitude test (c) Tensile test	1	123		99.98	
4	M1	(a) Temperature test (b) Altitude test (c) Humidity test	1	126		99.95	
5	M1	(a) Temperature test (b)Altitude test (c)Humidity test (d)Fluid test	1	141		99.98	
6	M2	(a)Temperature test (b)Altitude test	10	116	±27	99.96	±0.03
7	M2	(a) Temperature test (b) Altitude test (c) Fluid test	2	51	±35	99.98	±0.01
8	M2	(a) Temperature test (b) Altitude test (c) Tensile test	2	66	±6	99.97	±0.01
9	M2	(a) Temperature test (b) Altitude test (c) Humidity test (d) Vibrational test	4	75	±14	99.98	±0.01
10	M3	(a) Temperature test (b) Altitude test	12	147	±38	99.96	±0.04

ensure contact with the composite surface along the whole mounting length, for optimal strain transfer [34].

After applying a slightly excessive amount of X120 adhesive, we use a circle-segment cut-out made from aluminum, with dimensions of 2×5.64 mm to uniformly distribute the adhesive. A schematic of the resulting cross-section of a surface mounted SMW, *showing the outer circular geometry of the adhesive*, is illustrated in figure 7(a). By doing so, we ensure a uniform protective layer of adhesive surrounding and fixing the SMW. Note that the dimensions of the cut-out could be adapted if required. The dimensions used here ensured a complete covering of the SMW by the adhesive, as recommended elsewhere [35]. We pre-strained the SMWs with ~40 pm. In addition, the entire installation and curing occurred at 16 °C, ensuring an additional pre-strain of $133 - 152$ pm when operated or characterized at 23 °C $- 24$ °C, owing to the temperature sensitivity of 19 pm K^{-1}. This means that a total pre-strain of $173 - 192$ pm is applied on the bonded DTGs at room temperature. If the bond line were to fail, this means a negative wavelength shift of this order is expected. An image of two installed SMWs is shown in figure 7(b).

The application through a mixing nozzle allows for controlled and continuous dosing making it adaptable for automation. Moreover, the adhesive can be air-cured at room temperature, removing the need of an autoclave or oven,

although the curing time can be decreased considerably when increasing the curing temperature: from 29 h at 25 °C to just half an hour at 80 °C [33].

2.4. Coupon design

We used three different commonly used aerospace-grade carbon fibre reinforced polymer composite materials with specifications as in table 1, from now on referred to as M1, M2 and M3. Note that the third material is the same as the M1 material, but infused with carbon nanotubes (CNTs) acting as an electromagnetic shield. The in-plane dimensions of the composite coupons were 250×35 mm. Table 1 summarizes the lay-up for the three kinds of coupons. Essentially 19 M1 coupons, of which 12 with CNTs, and 9 M2 coupons were fabricated.

The M1 and M3 coupons were instrumented with one DTG per coupon, while the M2 material was instrumented with two DTGs per coupon. The layout of all coupons is shown in figure 8, with the dashed line denoting the area in which adhesive is applied.
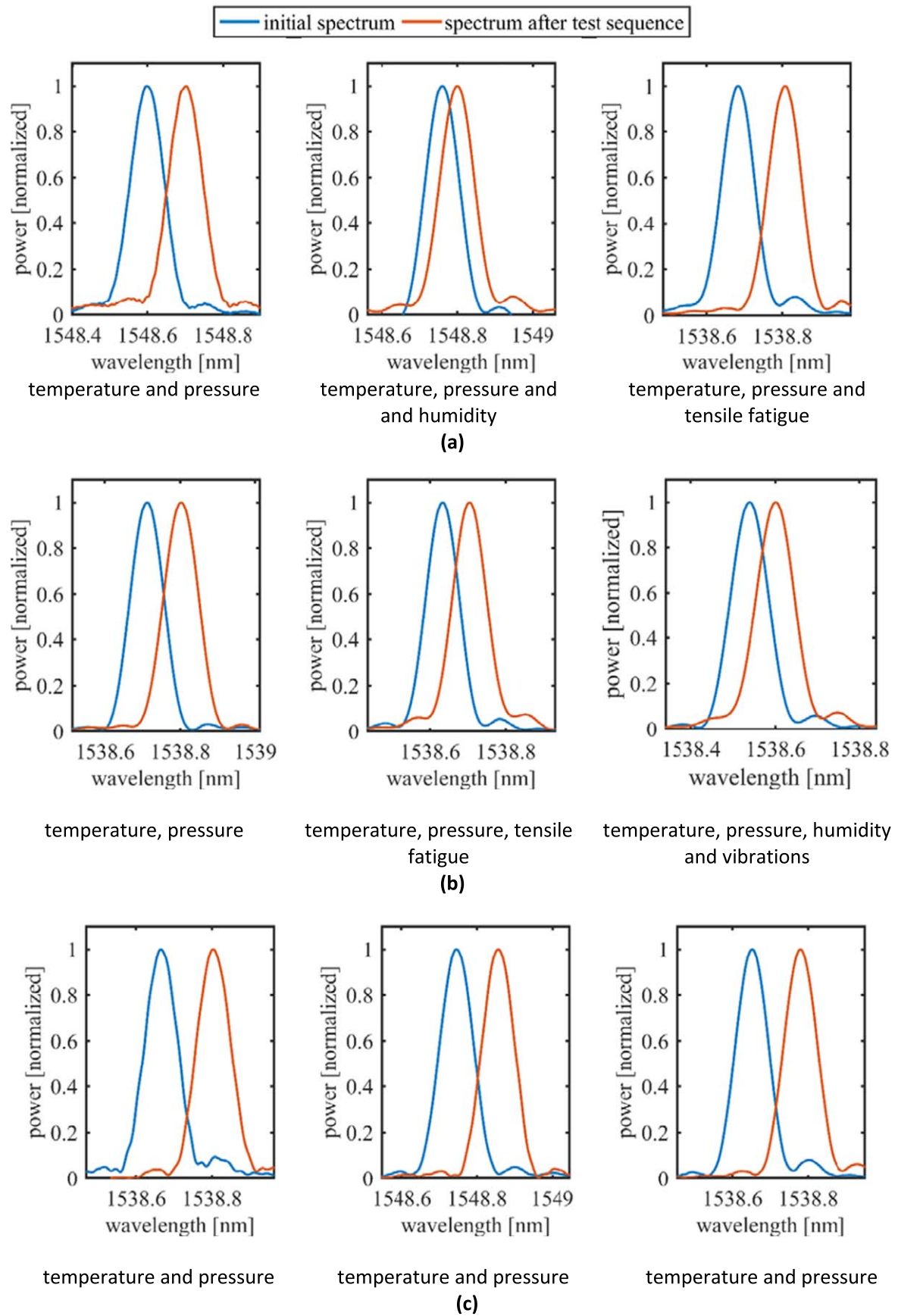
Figure 10. Bragg reflection spectra of the DTGs before and after the mentioned test for M1 (a), M2 (b), and M3 (c). Note that for calculating the correlation coefficient, the change in Bragg wavelength was neglected.

3. Experiments

3.1. Test parameters

To qualify the proposed sensors, the CFRP coupons with surface mounted SMW were tested against a full set of operational environment conditions based on RTCA/DO-160 environmental conditions and test procedures for airborne equipment and ASTM standards as summarized in table 2 [36].

All 28 coupons were exposed to temperature and sequentially to pressure conditions. We shock cycled the temperature conditions between maximum ground temperatures and typical in-flight conditions for 10 h. The profile can be seen in figure 9(a). The pressure test includes typical pressure conditions at sea level, at maximum cruising altitude, and in shock from one extreme to the other. The pressure profile can be found in figure 9(b). Typically temperature and pressure loading must be combined, but is was shown that sequential loading has the same effect [37].

Following the temperature and pressure tests, one or two other test conditions were applied to selections of the 28 coupons. Two M1 and four M2 DTGs were tested in high relative humidity (RH) for 48 h, while the temperature dropped twice at very low rate. The humidity/temperature profile for this test is depicted in figure 9(c). One M1 DTG and two M2 DTGs were tested for fluid susceptibility, by being submerged in a mineral hydraulic oil with very high level of cleanliness [38] for 24 h. Two M1 and four M2 DTGs were exposed to 1 h of random vibrations. The profile of this acceleration power spectral density (APSD) is illustrated in figure 9(d). For testing fatigue loading, one M1 and two M2 DTGs were submitted to 10^6 cycles of 5 kN ($R = 0.1$) tensile testing at 5 Hz based on ASTM D3497M, the Standard Test Method for Tension–Tension Fatigue of Polymer Matrix Composite Materials [39].

3.2. Results and discussion

Different test sequences have been considered and, each of those is mentioned in column three of table 3. After a coupon went through a particular test sequence, we acquired the spectra of the FBG sensor and compared it to the spectra of the installed sensor before testing.

We obtained the Bragg wavelength, by calculating the centroid of the Bragg peak in a 200 pm width around the maximum of the peak. This allows us to calculate the change in Bragg wavelength, $\Delta\lambda$, between the two spectral data sets. The average change in wavelength for all DTGs that went through the same set of tests, and their corresponding standard deviation σ, are displayed in column five and six of table 3 respectively.

If any of the applied loading conditions locally damages the sensor, the SMW coating or the adhesive bond line, this will result in a local non-uniform strain field around the 8 mm DTG and will distort the reflection spectrum of the Bragg peak. A complete debonding of the SMW would yield even higher non-uniform strain fields and thus distortions. Because we are interested here in the increase in distortion as a result of the tests, and not the distortion already present on the Bragg peak, we use the Pearson correlation coefficient in equation (2) to quantify the cross-correlation between the Bragg peak before and after the tests, neglecting the Bragg wavelength shift $\Delta\lambda$. In this case the x_i in (3) are the spectral data points of the Bragg peak prior to the exposure to the conditions, and y_i the spectral data points of the same sensor after the exposure. In both cases they are the spectral data points of a 200 nm window centering the Bragg wavelength, and normalized to the maximum height of the peak. The last two columns of table 3 display the average correlation for all DTGs going through the same set of tests and their standard deviation.

From the correlation coefficients in table 3, we conclude that the Bragg peaks obtained after any set of in-flight condition tests correlate very highly with the same peaks before the tests. This can be observed in figure 10, where a selection of reflection spectra before and after the tests is displayed. No noticeable change in the linearity or slope of the edge, or in FWHM can be observed. The lowest cross-correlation value, corresponding with the temperature and pressure testing of the SMW installed on M1, is indeed still as high as 99.94% ± 0.01%.

To evaluate these correlation coefficients, we applied the exact same analysis to the reflection spectra of 4 surface mounted SMW DTGs that were not exposed to any conditions. The reflection spectrum of each DTG was acquired three times, with ˜1 h in between measurements. The Pearson coefficient was calculated by correlating the first with the second, and the second with the third spectrum. The average of the resulting 8 correlation coefficients is $\rho = 99.96\% \pm 0.06\%$. This correlation coefficient is of the same order as those in table 3, so we can conclude that the effect of the in-flight loads on the distortion is indeed negligible, meaning that no noticeable non-uniform strain distribution is additionally acting on the 8 mm long DTG in the SMW, which suggests that the sensors are indeed not damaged, nor is the fibre coating, packaging or adhesive bond line locally affected. All DTG sensors, including their packaging and installation method remain operational and usable for high-frequency SHM, typically used in aerospace applications.

Moreover, table 3 shows only positive wavelength shifts which indicates that there is still pre-strain present on the SMWs. This further confirms that the adhesive bond line is not damaged. The positive wavelength shift is most likely attributed to a positive temperature difference of a few degrees, combined an effect of the tests on the composite material itself, as M1 (and M3) was on average more prone to this (average $\Delta\lambda$ of 119.27 pm) than M2 (average $\Delta\lambda$ of 76.83 pm).

4. Conclusion

In this work we proposed a specialty coated fibre Bragg grating, called the SMW, and demonstrated its compatibility

with in-flight conditions when adequately surface-mounted on aerospace grade CFRP coupons.

We equipped 28 aerospace-grade CFRP coupons with SMWs and exposed them to a set of standardized in-flight conditions involving temperature, pressure and humidity tests, but also APSD vibration, susceptibility to hydraulic fluid and tensile fatigue. We compared the spectra of the FBGs before and after the tests and evaluated distortion of the Bragg peaks, and the change in Bragg wavelength in a 200 pm window. No noticeable effect was observed on the quality of the DTG reflection spectra. Moreover, all FBGs were still pre-strained after the tests.

We conclude that the DTG sensors, the packaging and its installation method were negligibly affected by any of the applied in-flight conditions and the SMWs remain fully operational. This result supports the applicability of FBG-based sensors for SHM strategies in aerospace-grade composite structures, such as for example ultrasound-based damage identification or techniques based on modal analysis.

Acknowledgments

ORCID iDs

Sidney Goossens https://orcid.org/0000-0002-3371-8647
Ben De Pauw https://orcid.org/0000-0002-9606-0483
Thomas Geernaert https://orcid.org/0000-0002-8195-8071
Diego Saenz-Castillo https://orcid.org/0000-0003-4378-1452
Hugo Thienpont https://orcid.org/0000-0003-0483-0960
Francis Berghmans https://orcid.org/0000-0003-0822-233X

References

[1] Abbas S, Li F and Qiu J 2018 A review on SHM techniques and current challenges for characteristic investigation of damage in composite material components of aviation industry *Mater. Perform. Charact.* **7** 20170167

[2] Sante R D 2015 Fibre optic sensors for structural health monitoring of aircraft composite structures: recent advances and applications *Sensors* **15** 18666–713

[3] De Waele W, Degrieck J, Moerman W, Taerwe L and Baets P D 2003 Feasibility of integrated optical fibre sensors for condition monitoring of composite structures: I. Comparison of Bragg-sensors and strain gauges *Insight-Non-Destr. Test. Cond. Monit.* **45** 266–71

[4] Groves R M, Chehura E, Li W, Staines S E, James S W and Tatam R P 2007 Surface strain measurement: a comparison of speckle shearing interferometry and optical fibre Bragg gratings with resistance foil strain gauges *Meas. Sci. Technol.* **18** 1175–84

[5] Mrad N, Sparling S and Laliberte J 1999 Strain monitoring and fatigue life of Bragg grating fiber optic sensors *1999 Symp. on Smart Structures and Materials* pp 82–91

[6] Jensen D W and Pascual J 1990 Degradation of graphite/bismaleimide laminates with multiple embedded fiber optic sensors *Proc. SPIE* 1370, 228–38

[7] Lee D C, Lee J J and Yun S J 1995 The mechanical characteristics of smart composite structures with embedded optical fiber sensors *Compos. Struct.* **32** 39–50

[8] Satori K, Fukuchi K, Kurosawa Y, Hongo A and Takeda N 2001 Polyimide-coated small-diameter optical fiber sensors for embedding in composite laminate structures *Proc. SPIE* **4328** 285–95

[9] Shivakumar K and Emmanwori L 2004 Mechanics of failure of composite laminates with an embedded fiber optic sensor *J. Compos. Mater.* **38** 669–80

[10] Luyckx G, Voet E, Lammens N and Degrieck J 2010 Strain measurements of composite laminates with embedded fibre Bragg gratings: criticism and opportunities for research *Sensors* **11** 384–408

[11] Dawood T A, Shenoi R A and Sahin M 2007 A procedure to embed fibre Bragg grating strain sensors into GFRP sandwich structures *Compos. Part Appl. Sci. Manuf.* **38** 217–26

[12] Lu S and Xie H 2007 Strengthen and real-time monitoring of RC beam using 'intelligent' CFRP with embedded FBG sensors *Constr. Build. Mater.* **21** 1839–45

[13] 'Optical Strain Sensors FS62,' HBM, 16 April 2018 https://hbm.com/en/4600/fs62-optical-strain-sensor-fibersensing/ (accessed: 07 January 2019)

[14] Bosboom M *et al* 2016 Ribbon tapes, shape sensors, and hardware *Proc. Smart Intelligent Aircraft Structures (SARISTU)* ed P C Wölcken and M Papadopoulos pp 349–4069783319224138

[15] Loutas T H, Charlaftis P, Airoldi A, Bettini P, Koimtzoglou C and Kostopoulos V 2015 Reliability of strain monitoring of composite structures via the use of optical fiber ribbon tapes for structural health monitoring purposes *Compos. Struct.* **134** 762–71

[16] Nedjalkov A *et al* 2018 Direct inscription and evaluation of fiber Bragg gratings in carbon-coated optical sensor glass fibers for harsh environment oil and gas applications *Appl. Opt.* **57** 7515

[17] Wnuk V P, Mendez A, Ferguson S and Graver T 2005 Process for mounting and packaging of fiber Bragg grating strain sensors for use in harsh environment applications *Proc. SPIE Smart Structures and Materials 2005: Smart Sensor Technology and Measurement Systems* 5758, 46

[18] FBGS International, Strain Measurement Wire SMW-1 https://fbgs.com/productsadv/be-en/5/detail/item/31/page/1/

[19] Goossens S, De Pauw B, Geernaert T, Salmanpour M.S., Sharif Khodaei Z, Thienpont H and Berghmans F 2018 Aerospace-grade compatible surface mounted optical fibre sensor for structural health monitoring of composite structures *Advanced Photonics 2018 (BGPP, IPR, NP, NOMA, Sensors, Networks, SPPCom, SOF) (Zurich)* p BM3A.5

[20] Kashyap R 1999 *Fiber Bragg Gratings* (New York: Academic) 978-0-12-400560-0

[21] Othonos A 2000 Bragg gratings in optical fibers: fundamentals and applications *Optical Fiber Sensor Technology* ed K T V Grattan and B T Meggitt (US: Springer) pp 79–187

[22] Erdogan T 1997 Fiber grating spectra *J. Light. Technol.* **15** 1277–94

[23] Krohn David. A., MacDougall Trevor W. and Mendez Alexis 2015 *Fiber Optic Sensors: Fundamentals and Applications, Fourth Edition* (United States: SPIE press) 9781628411805

[24] Culshaw B, Thursby G, Betz D and Sorazu B 2008 The detection of ultrasound using fiber-optic sensors *IEEE Sens. J.* **8** 1360–7

[25] Betz D C, Thursby G, Culshaw B and Staszewski W J 2003 Acousto-ultrasonic sensing using fiber Bragg gratings *Smart Mater. Struct.* **12** 122

[26] Perez I M, Cui H and Udd E 2001 Acoustic emission detection using fiber Bragg gratings *SPIE's 8th Annual Int. Symp. on Smart Structures and Materials (Newport Beach, CA)* p 209

[27] Panopoulou A, Loutas T, Roulias D, Fransen S and Kostopoulos V 2011 Dynamic fiber Bragg gratings based health monitoring system of composite aerospace structures, *Acta Astronaut.* **69** 445–57

[28] Frieden J, Cugnoni J, Botsis J, Gmür T and Ćorić D 2010 High-speed internal strain measurements in composite structures under dynamic load using embedded FBG sensors *Compos. Struct.* **92** 1905–12

[29] Peters K, Studer M, Botsis J, Iocco A, Limberger H and Salathé R 2001 Embedded optical fiber Bragg grating sensor in a nonuniform strain field: measurements and simulations *Exp. Mech.* **41** 19–28

[30] FBGS International 2015 Draw tower gratings, http://www.fbgs.com/

[31] Johnson D 2012 Draw-tower process creates high-quality FBG arrays *Laser Focus World* **48** 53–56

[32] Mihailov S J 2012 Fiber Bragg grating sensors for harsh environments *Sensors* **12** 1898–918

[33] X120 Adhesive for the Installation of Optical FBG Sensors, *HBM*, 21 November 2018 https://hbm.com/en/2489/strain-gauges-adhesives-x120-two-component-adhesive/ (accessed: 18 December 2018)

[34] Wan K T, Leung C K Y and Olson N G 2008 Investigation of the strain transfer for surface-attached optical fiber strain sensors *Smart Mater. Struct.* **17** 035037

[35] De Pauw B, Vanlanduit S, Van Tichelen K, Geernaert T, Chah K and Berghmans F 2013 Benchmarking of deformation and vibration measurement techniques for nuclear fuel pins *Measurement* **46** 3647–53

[36] U.S. Department of Transportation, Federal Aviation Administration 2005 *RTCA, Inc. Document RTCA/DO-160E, Environmental Conditions and Test Procedures for Airborne Equipment* (United States: U.S. Department of Transportation, Federal Aviation Administration)

[37] Salmanpour M, Sharif Khodaei Z and Aliabadi M 2016 Airborne transducer integrity under operational environment for structural health monitoring *Sensors* **16** 2110

[38] 'The AeroShell Book.' https://shell.com/business-customers/aviation/aeroshell/knowledge-centre/the-aeroshell-book.html (accessed: 08 January 2019)

[39] ASTM international 2019 D60: Test Method for Tension–Tension Fatigue of Polymer Matrix Composite Materials *Annual Book of ASTM Standards* (United States: ASTM International)